RSC Advances

PAPER

View Article Online
View Journal | View Issue

Cite this: *RSC Adv.*, 2018, **8**, 12791

Ascorbic acid/Fe^0 composites as an effective persulfate activator for improving the degradation of rhodamine B

Xiangyu Wang, *[a] Yi Du,[a] Huiling Liu[b] and Jun Ma[b]

An ascorbic acid/Fe^0 composite (H_2A/Fe^0)-activated persulfate (PS) process was provided for rhodamine B (RhB) removal. Experimental results demonstrated that the H_2A/Fe^0–PS system exhibits a rapid and continuous oxidation of organic contaminants, and shows great advantages over the conventional Fe^0–PS system by significantly improving removal efficiency. This H_2A induced dramatic enhancement for RhB degradation could be attributed to both the reduction and chelating ability of H_2A. The H_2A/Fe^0 composites were characterized using TEM, FE-SEM, FTIR and XPS, indicating that the obtained H_2A/Fe^0 composites were prepared successfully. Key factors affecting the treatment were determined for the H_2A/Fe^0–PS system, including H_2A/Fe^0 dosage, PS dosage, initial solution pH and temperature. Moreover, radical quenching tests revealed that sulfate radicals ($SO_4^{\bullet-}$), hydroxyl radicals ($^{\bullet}OH$) and superoxide radicals ($O_2^{\bullet-}$) were generated in the H_2A/Fe^0–PS system, and $SO_4^{\bullet-}$ was the main radical species responsible for RhB degradation. Finally, possible degradation pathways are proposed. These findings prove that the H_2A/Fe^0–PS system may provide a simple and effective technology for improving the degradation of refractory organic pollutants.

Received 19th February 2018
Accepted 26th March 2018

DOI: 10.1039/c8ra01506f

rsc.li/rsc-advances

1. Introduction

Nowadays, advanced oxidation processes (AOPs) are regarded as good alternatives for the *in situ* oxidation of various organic pollutants.[1] In particular, sulfate radical ($SO_4^{\bullet-}$, $E_0 = 2.5$–3.1 V) based AOPs have become hot topics of research due to their high oxidizing ability, wide pH range and long lifetime.[2] The highly reactive $SO_4^{\bullet-}$ can be generated by activation of persulfate (PS) with heat,[3] UV,[4] metal oxides (Fe_3O_4, $CuFe_2O_4$),[5,6] or transition metals (*e.g.*, Fe^{2+}, Co^{2+}, Cu^{2+}).[7,8] Among these methods, Fe^{2+} has been commonly selected as the activator for PS to generate $SO_4^{\bullet-}$ *via* eqn (1) due to its non-toxicity, low cost and abundance.[9] However, in the Fe^{2+}/PS system, Fe^{2+} is hard to regenerate after conversion to Fe^{3+}. In addition, excess Fe^{2+} will scavenge the generated $SO_4^{\bullet-}$ *via* eqn (2), resulting in reduced degradation efficiency for target contaminants.

$$S_2O_8^{2-} + Fe^{2+} \rightarrow SO_4^{\bullet-} + Fe^{3+} + SO_4^{2-} \quad (1)$$

$$SO_4^{\bullet-} + Fe^{2+} \rightarrow Fe^{3+} + SO_4^{2-} \quad (2)$$

Zero-valent iron (Fe^0) can be an alternative source of Fe^{2+} by gradually releasing Fe^{2+} into an aqueous solution so that Fe^{2+} induced scavenging is minimal.[10] Moreover, in the Fe^0/PS system, Fe^0 can not only lessen the generation of ferric hydroxides by recycling Fe^{3+} at the surface of ZVI *via* eqn (3), but also directly transfer electrons to PS, resulting in the generation of $SO_4^{\bullet-}$ *via* eqn (4). Peluffo *et al.* reported that the Fe^0/PS process yielded a higher removal rate of PAHs than the Fe^{2+}–PS process under optimal conditions.[11]

$$Fe^{3+} + Fe^0 \rightarrow Fe^{2+} \quad (3)$$

$$S_2O_8^{2-} + Fe^0 \rightarrow 2SO_4^{\bullet-} + Fe^{2+} + 2SO_4^{2-} \quad (4)$$

Recently, an Fe^0–PS system has been employed to remove various organic pollutants, such as trichloroethylene (TCE),[12] orange G (OG),[13] and bentazon (BTZ).[10] However, the biggest drawback of this technology is that it requires high concentrations of PS and Fe^0 dosages to achieve favorable activation performance, resulting in increased treatment cost and extra disposal,[14] which may be due to the slow conversion from Fe^{3+} to Fe^{2+}.[15] Therefore, accelerating the redox cycle of Fe^{3+}/Fe^{2+} is crucial to improving the oxygen activation performance of the Fe^0–PS system for practical application.

To solve the above-mentioned problems, we conducted a new attempt to provide a novel ascorbic acid/Fe^0–PS system to degrade organic pollutants in an aqueous system. In this research work, Fe^{3+}/Fe^{2+} cycles were successfully promoted by employing a reducing agent, ascorbic acid ($C_6H_8O_6$, H_2A), in the Fe^0–PS system. Ascorbic acid (H_2A), which is also known as

[a]*Faculty of Environmental Science and Engineering, Kunming University of Science and Technology, Kunming 650500, P. R. China. E-mail: imusthlee2014@sina.com*
[b]*School of Municipal and Environmental Engineering, State Key Laboratory of Urban Water Resources and Environment, Harbin Institute of Technology, Harbin 150090, P. R. China*

vitamin C, is an eco-friendly reducing agent and a natural antioxidant. H_2A has shown great promise in water and wastewater treatment.[16] Many high oxidation states like H_2O_2, Fe^{3+}, and Cr^{6+} could be reduced using H_2A as an electron donor.[17,18] Fukuchi *et al.* reported that the dosages of H_2O_2 and Fe^{2+} could be largely reduced with the addition of H_2A into traditional Fenton-like processes, leading to a relatively steady Fe^{2+} concentration and higher production of free radicals.[19] In addition, H_2A is a bidentate ligand with a bifunctional enediol group that has the ability to solubilize metal ions by chelate formation.[20] Therefore, it might be reasonable to introduce H_2A into the Fe^0–PS system to improve the degradation efficiency for pollutants. Although it has also been reported that Fe^0 nanoparticles can be stabilized with ascorbic acid to increase the durability of synthesized Fe^0.[21] To the best of our knowledge, the use of H_2A coated Fe^0 nanoparticles as an activator to enhance the activation performance of PS has not been reported so far.

To investigate the degradation efficiency of the H_2A/Fe^0–PS system, rhodamine B (RhB) was selected as a model pollutant because it is an extremely stable and resistant aromatic compound, and hard to degrade using conventional wastewater treatment methods. The additional purposes of this study were to (1) investigate the degradation performance of RhB in the H_2A/Fe^0–PS system; (2) explore the mechanism of enhanced RhB degradation in the H_2A/Fe^0–PS system; and (3) reveal the important parameters (H_2A/Fe^0 dosage, PS dosage, pH and temperature) affecting the H_2A/Fe^0–PS system.

2. Materials and methods

2.1. Chemicals and materials

Potassium borohydride (KBH_4, 99%), ferrous sulfate heptahydrate ($FeSO_4 \cdot 7H_2O$), sodium persulfate ($Na_2S_2O_8$), sodium hydroxide (NaOH, 99%), rhodamine B (RhB), sulfuric acid (H_2SO_4, 95% to 98%), sodium acetate anhydrous (CH_3COONa), ethanol, 1,10-phenanthroline ($C_{12}H_8N_2$), *tert*-butyl alcohol (TBA), methanol (MeOH), 1,4-benzoquinone (BQ), acetone and ascorbic acid (H_2A) were of analytical grade and purchased from Sinopharm Chemical Reagent Co., Ltd. All the solutions were prepared with deionized water before each run.

2.2. Synthesis of H_2A/Fe^0

The H_2A/Fe^0 was synthesized in an anaerobic glove box under the protection of purified N_2. First, a 0.5 M solution of Fe^{2+} was prepared by dissolving $FeSO_4 \cdot 7H_2O$ in deionized water (100 mL). Then, a certain volume stabilizer (H_2A, 10 g L^{-1}) solution was added into the $FeSO_4$ solution with electromagnetic stirring for 15 min. After intensive mixing, 100 mL of 1.5 M of KBH_4 solution was added dropwise into the mixture solution. After delivering all of the KBH_4 solution, the solution was stirred continuously for 30 min. Subsequently, the solid precipitation was filtered with a 0.45 μm membrane filter under vacuum, followed by rinsing with deionized water, absolute ethanol, and acetone alternately 3 times.

2.3. Experimental procedures

Degradation experiments were carried out in 250 mL serum bottles, which were filled with 50 mL of RhB solution. A predetermined amount of PS was quickly added into the pH-adjusted RhB solution. Subsequently, a certain amount of H_2A/Fe^0 was quickly added into the above solution to trigger the reaction. The initial pH value of the solution was adjusted with NaOH (0.1 M) or H_2SO_4 (0.1 M). The bottles were then placed into a temperature-controlled orbital shaker with a constant shaking speed (170 rpm) to ensure a complete mixing state. At predetermined time intervals, solution samples were taken using disposable syringes, and then filtered with a 0.45 μm filter membrane. Subsequently, the filtered sample was mixed with excess methanol (v/v = 1 : 1) to quench the reaction before analysis.

The concentration of RhB was determined with a UV-2450 visible spectrophotometer (Shimadzu, Japan), and its maximum characteristic wavelength was adopted at 554 nm. The concentrations of total iron and ferrous ions were determined according to the 1,10-phenanthroline colorimetric method.[22] Radical scavenging tests were conducted and three radical scavengers, MeOH, TBA and BQ, were used to determine the type of the predominant reactive oxygen species for RhB degradation.

2.4. Characterizations

The morphology and particle structure of H_2A/Fe^0 and Fe^0 were studied with a high-resolution field emission scanning electron microscope (FE-SEM, JEOL Ltd., Japan) at an accelerating voltage of 5.0 kV with an X-ray energy-dispersive spectroscopy (EDS) detector (IE300X, Oxford, United Kingdom) and transmission electron microscopy (TEM, JEOL Ltd., Japan). The surface chemical structure and composition of the H_2A/Fe^0 and Fe^0 particles were studied by Fourier transform infrared spectroscopy (FTIR, Perkin-Elmer Instrument Co. Ltd., USA). The element valence and chemical groups of H_2A/Fe^0 and Fe^0 were determined by X-ray photoelectron spectroscopy using monochromatic Mg Kα radiation (XPS, Model PHI 5700, Physical Electronics, USA).

3. Results and discussion

3.1. Comparison of RhB degradation in different systems

Comparative experiments were carried out in different systems to determine the effects of the synthesized H_2A/Fe^0 particles on PS activation for RhB degradation under the same operating conditions. As shown in Fig. 1a, about 35.28% RhB was removed by Fe^0 alone, and only 31.33% RhB was removed by H_2A/Fe^0 within 90 min, indicating that some of the reactive sites might be blocked by the excessive dispersant coated on the Fe^0 surfaces. The removal efficiency for RhB was apparently improved when the reaction time was prolonged, mainly because of desorption of H_2A into the aqueous solution. In contrast, PS alone could degrade 54.59% of RhB within 90 min. The carboxyl and phenyl groups of RhB might be capable of PS activation.[23] In addition, activation of PS by Fe^0 was also

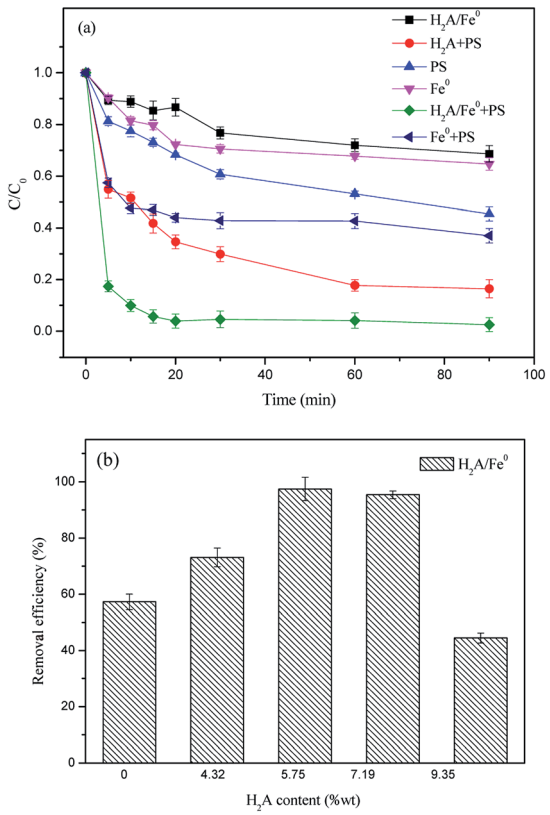

Fig. 1 (a) Comparison of removal efficiency of RhB in different systems (C_0 = 50 mg L^{-1}, PS dosage = 1.4 g L^{-1}, Fe^0 dosage = 1 g L^{-1}, H_2A/Fe^0 dosage = 1 g L^{-1}, H_2A dosage = 1.6 g L^{-1} and T = 298 K); (b) effect of H_2A concentration on removal efficiency of RhB in the H_2A/Fe^0–PS system (C_0 = 50 mg L^{-1}, Fe^0 dosage = 0.8 g L^{-1}, T = 298 K and the solution volume is 50 mL).

investigated, and the results showed that approximately 18% of the RhB was removed over 60 min in the Fe^0/PS system. A slightly improved removal efficiency of RhB was achieved in the H_2A/PS system because H_2A can react with PS to generate $SO_4^{\cdot-}$, according to eqn (5) and (6).[24] However, more than 90% of the RhB was removed with H_2A/Fe^0 activated PS. Therefore, the high activity of the H_2A/Fe^0 composites for PS activation was assumed to be the result of the existence of a synergistic effect in this system.

$$H_2A + S_2O_8^{2-} \rightarrow 2H^+ + SO_4^{2-} + SO_4^{\cdot-} + A^{\cdot-} \quad (5)$$

$$HA^- + S_2O_8^{2-} \rightarrow H^+ + SO_4^{2-} + SO_4^{\cdot-} + A^{\cdot-} \quad (6)$$

The reactivity of H_2A/Fe^0 particles with different H_2A content was further investigated. As shown in Fig. 1b, the highest removal efficiency was achieved with an H_2A solution addition amount of 3.60‰ wt (to Fe^{2+}) during the synthesis process of Fe^0. For an H_2A addition content higher than 3.60‰, the excess H_2A might occupy the available reactive sites of Fe^0 particles and then block the target pollutants diffusing onto the surface sites. In contrast, insufficient loading of the coating onto the surface of Fe^0 might result in ineffective dispersion of the Fe^0, indicating that the optimal H_2A concentration would be 3.60‰. Therefore, 3.60‰ was selected in the following characterization and degradation experiments.

3.2. Characterization of H_2A/Fe^0

The morphology of the Fe^0 and H_2A/Fe^0 was observed by TEM and FE-SEM. The TEM observation (Fig. 2a) on the Fe^0 shows that bare Fe^0 particles were aggregated and featured as a necklace-like chain of length 80–100 nm. When H_2A was added, the dispersion of Fe^0 was significantly increased (Fig. 2b), indicating that H_2A could act as a dispersant for Fe^0 nanoparticles. The particle size of H_2A/Fe^0 ranges from 20 to 80 nm. The reason might be that the added H_2A could coordinate with ferrous ions to indirectly control the growth of iron particles, resulting in the smaller size of the H_2A/Fe composite.

Fig. 2c shows the representative FE-SEM image of the as-synthesized bare Fe^0, which exhibits a spherical morphology with a size in the range 80–100 nm, and which tends to aggregate together due to the magnetic interactions between iron particles.[21] Comparatively, with the coating of H_2A, it can be observed that the H_2A/Fe^0 had a smaller size than bare Fe^0 (Fig. 2d). Simultaneously, the EDS spectrum further revealed the successful incorporation of H_2A and iron nanoparticles (Fig. 3e).

In order to prove the existence of functional groups of H_2A on the surface of the Fe nanoparticles, Fe^0 and H_2A/Fe^0 were analyzed by FTIR spectroscopy. As shown in Fig. 3, the absorption peak on H_2A/Fe^0 at about 3417 cm^{-1} was significantly larger than that on Fe^0, which was attributed mainly to stretching vibrations of –OH.[25] In addition, compared with the

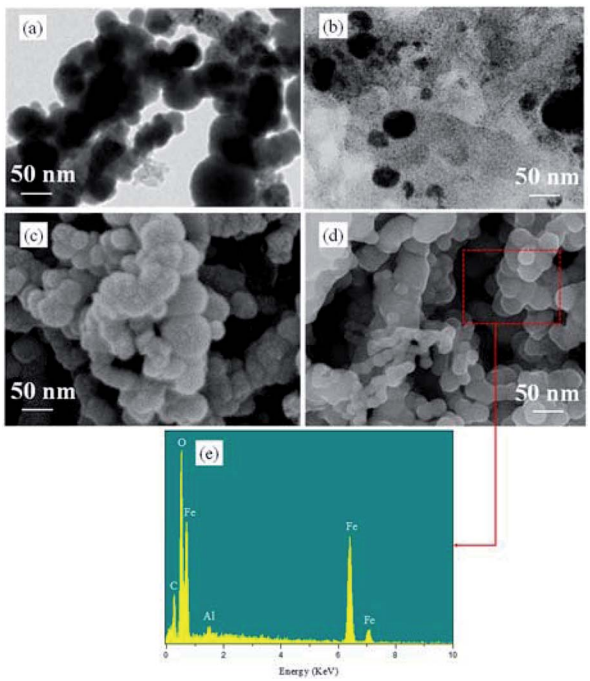

Fig. 2 TEM images of (a) Fe^0 and (b) H_2A/Fe^0, FE-SEM images of (c) Fe^0 and (d) H_2A/Fe^0, and (e) electron diffusion spectroscopy elemental analysis.

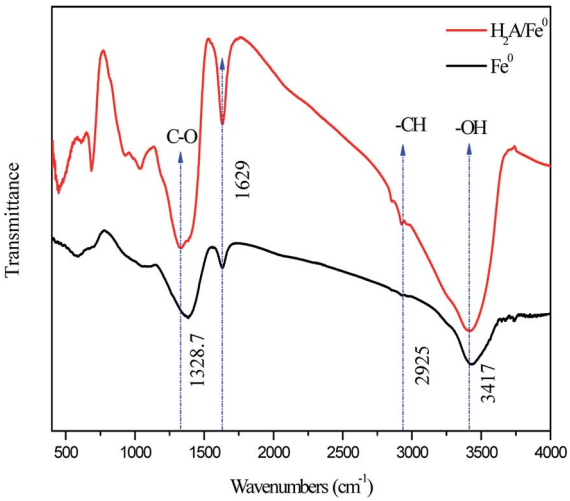

Fig. 3 FTIR spectra of Fe^0 and H_2A/Fe^0.

spectrum of Fe^0, there are several inconspicuous infrared characteristic peaks for H_2A/Fe^0, among which the absorption peak appearing at approximately 2925 cm^{-1} was assigned to –CH. The bands at 1328.7 cm^{-1} are attributed to C–O vibrations. Meanwhile, an additional adsorption peak at 1629 cm^{-1} corresponded to the stretching vibrations of C=C groups, indicating the presence of the H_2A constituent.[15]

XPS was used to investigate the composition and chemical state of Fe^0 before and after coating by H_2A. The full-range survey spectra of Fe^0 and H_2A/Fe^0 particles are illustrated in Fig. 4a, showing that the nanoparticle surface consists mainly of iron (Fe), oxygen (O), and carbon (C). The small amount of carbon appearing in the Fe^0 spectrum is likely to be attributed to carbon dioxide, water, and/or organic compounds (such as ethanol and acetone) during the fabrication, drying and preserving processes.[26] Detailed XPS patterns for the C 1s regions of the Fe^0 and H_2A/Fe^0 particles are presented in Fig. 4b and c. Compared with Fe^0, a conspicuous peak at 284.7 eV appeared in the spectrum of H_2A/Fe^0, corresponding to C=C species, verifying the presence of H_2A. All the above characterization results of FTIR and XPS confirmed that H_2A had been successfully coated onto Fe^0.

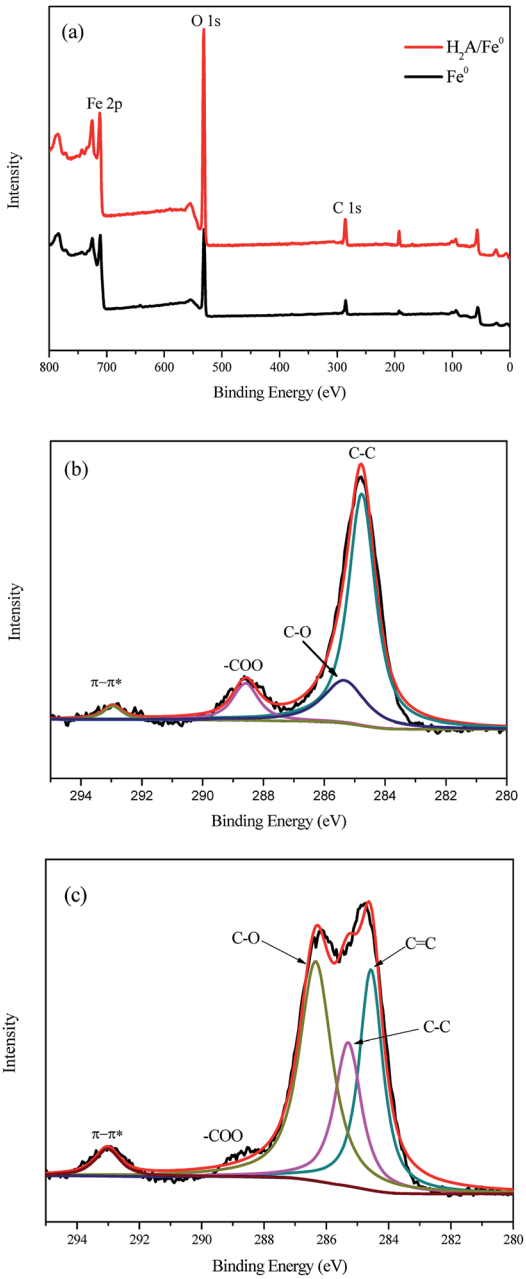

Fig. 4 XPS spectra of Fe^0 and H_2A/Fe^0: (a) full-range XPS spectra, (b) C 1s regions of Fe^0, and (c) C 1s regions of H_2A/Fe^0.

3.3. Factors affecting RhB degradation in the H_2A/Fe^0–PS system

The effects of PS dosage, H_2A/Fe^0 dosage, pH value, and temperature on RhB degradation were investigated and the results are shown in Fig. 5. Fig. 5a shows the effect of PS dosage on RhB degradation. The results clearly show that the degradation of RhB accelerated as the PS dosage increased from 0.1 to 0.3 g L^{-1}. Since PS was the $SO_4^{\bullet -}$ donor, a higher PS dosage would improve the formation of $SO_4^{\bullet -}$. However, when the PS dosage was further increased to 0.5 g L^{-1}, it led to a decline in RhB degradation efficiency. Similar results were also reported in other studies.[27] A reasonable explanation for this phenomenon is that the excess $S_2O_8^{2-}$ may lead to $SO_4^{\bullet -}$ scavenging (eqn (7)) and the reaction between two $SO_4^{\bullet -}$ (eqn (8)).[28] Hence, 0.3 g L^{-1} PS was selected as the optimal dosage in the following experiments.

$$SO_4^{\bullet -} + S_2O_8^{2-} \rightarrow SO_4^{2-} + S_2O_8^{\bullet -} \quad (7)$$

$$SO_4^{\bullet -} + SO_4^{\bullet -} \rightarrow S_2O_8^{\bullet -} \quad (8)$$

The effect of H_2A/Fe^0 dosage on RhB degradation was evaluated with the H_2A/Fe^0 dosage ranging from 0.15 to 0.60 g L^{-1}. As shown in Fig. 5b, the increase in the activator dosage significantly promoted the degradation of RhB, which may be because the increase in H_2A/Fe^0 dosage could provide more

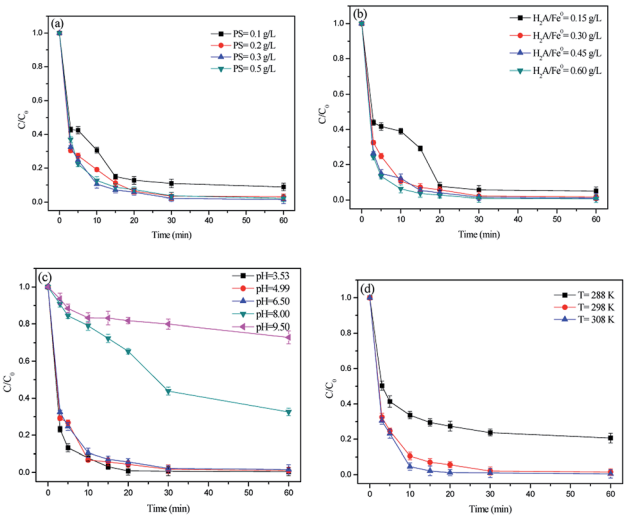

Fig. 5 Parameters affecting the degradation of RhB: (a) PS dosage, (b) H_2A/Fe^0 dosage, (c) pH value, and (d) temperature. Except for the investigated parameter, other parameters were fixed at C_0 = 50 mg L^{-1}, PS = 0.3 g L^{-1}, H_2A/Fe^0 = 0.3 g L^{-1}, pH = 6.50 and T = 298 K.

active sites for the activation of PS, thus producing more reactive free radicals for more efficient RhB degradation. At a lower dosage of H_2A/Fe^0 (0.15 g L^{-1}), 94.44% removal could be obtained within 30 min, indicating the excellent activity of H_2A/Fe^0 for PS activation with 50 mg L^{-1} RhB.

Fig. 5c shows the RhB degradation in the H_2A/Fe^0–PS system with different initial pH values ranging from 3.53 to 9.50. The pH value played an important parameter in the degradation of contaminants.[29] It could be observed that the highest RhB removal was achieved at an initial pH value of 3.53, and the removal efficiency obviously increased as the pH value decreased. This result is in accordance with Leng *et al.*'s report, which suggested that the degradation rate was lowered under neutral and alkaline conditions.[30] The better performance under acidic conditions in the present study may be because: (1) At lower pH values, the Fe^0 corrosion rate could be accelerated, leading to much faster release of Fe^{2+}, which favors the induction of eqn (1) to produce more $SO_4^{\bullet-}$. (2) At a pH higher than 7, the formation of Fe^{2+} complexes could inhibit PS activation by eqn (9). Also, the reactions between $SO_4^{\bullet-}$ and H_2O/OH^- could result in the rapid decay of $SO_4^{\bullet-}$ (eqn (10) and (11)).[31] Overall, acidic and weakly alkaline conditions were beneficial for RhB destruction. Compared with the Fenton process that must be carried out over a narrow pH range, the results suggested that the novel method we provide in this research possesses tremendous advantages for applications in practice.

$$Fe^{2+} + H_2O \rightarrow FeOH^+ + H^+ \quad (9)$$

$$\text{All pH: } SO_4^{\bullet-} + H_2O \rightarrow {}^{\bullet}OH + SO_4^{2-} + H^+ \quad (10)$$

$$\text{Alkaline pH: } SO_4^{\bullet-} + OH^- \rightarrow {}^{\bullet}OH + SO_4^{2-} \quad (11)$$

The degradation reaction of RhB was also found to be influenced by solution temperature. As shown in Fig. 5d, higher temperatures favored the degradation of RhB by PS activated with H_2A/Fe^0, which could be associated with the thermal activation of PS to generate free radicals (eqn (12)),[32] as well as the acceleration of the reaction between H_2A/Fe^0 and PS, probably because the diffusion and mobility of RhB molecules increased.

$$S_2O_8^{2-} + \text{heat} \rightarrow SO_4^{\bullet-} \quad (12)$$

3.4. Degradation mechanism

3.4.1 Identification of free radicals in the H_2A/Fe^0–PS system. It has been reported that a series of reactive oxygen species, *e.g.*, $SO_4^{\bullet-}$, $^{\bullet}OH$ and superoxide anion radicals ($O_2^{\bullet-}$), were generated in a PS/Fe(II)/hydroxylamine (HA) system and may also be generated in the H_2A/Fe^0–PS system.[33] In order to evaluate the major radical species for the RhB oxidation reaction, scavenging experiments were performed in the H_2A/Fe^0–PS system by adding MeOH, TBA and BQ into the reaction solution. MeOH (with α-hydrogen) is an effective quencher for both $^{\bullet}OH$ (1.2×10^9 to 2.8×10^9 M^{-1} s^{-1}) and $SO_4^{\bullet-}$ (1.6×10^7 to 7.7×10^7 M^{-1} s^{-1}). In contrast, TBA (without α-hydrogen) has an approximately 1000 times greater rate constant with $^{\bullet}OH$ (3.8×10^8 to 7.6×10^8 M^{-1} s^{-1}) than with $SO_4^{\bullet-}$ (4.0×10^5 to 9.1×10^5 M^{-1} s^{-1}).[6,34] Therefore, MeOH was used to scavenge both radicals, and TBA was used to selectively scavenge $^{\bullet}OH$. Moreover, we used BQ as an effective scavenger of $O_2^{\bullet-}$ by electron transfer to generate benzoquinone radicals.[35]

As shown in Fig. 6, 94.78% of RhB was degraded in 30 min when no quenching agent was added. However, with the addition of BQ and TBA, the removal efficiency of RhB decreased to 82.44% and 64.63% in 30 min, respectively. Meanwhile, the degradation of RhB was almost completely inhibited (27.98%) by the addition of MeOH. These data indicate that $O_2^{\bullet-}$, $SO_4^{\bullet-}$ and $^{\bullet}OH$ are generated in the H_2A/Fe^0–PS system. Similar findings were reported by a previous study.[36] It can be preliminarily inferred that $O_2^{\bullet-}$ may be derived from catalytic hydrolysis of PS

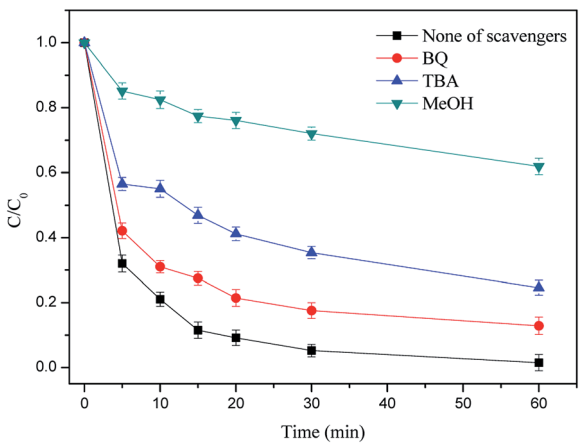

Fig. 6 Effect of different radical quenching agents on RhB removal. Reaction conditions: C_0 = 50 mg L^{-1}, PS = 0.3 g L^{-1}, H_2A/Fe^0 = 0.3 g L^{-1}, pH = 6.50 and T = 298 K.

in accordance with eqn (13) and (14). Hence, the scavenging studies clearly prove the simultaneous participation of $O_2^{\bullet-}$, $SO_4^{\bullet-}$ and $^{\bullet}OH$ in the H_2A/Fe^0–PS oxidation process, and $SO_4^{\bullet-}$ played a major role in achieving a good oxidation reaction.

$$S_2O_8^{2-} + 2H_2O \rightarrow 2SO_4^{2-} + HO_2^- + 3H^+ \quad (13)$$

$$S_2O_8^{2-} + HO_2^- \rightarrow SO_4^{2-} + SO_4^{\bullet-} + O_2^{\bullet-} + H^+ \quad (14)$$

3.4.2 UV-vis spectral changes. The UV-vis spectra were used to observe changes during the degradation of RhB by the H_2A/Fe^0–PS system at different reaction times. As shown in Fig. 7, there were two main characteristic absorption bands of RhB in the UV region (259 nm) and visible light region (554 nm), respectively. The UV absorbance at 259 nm corresponds to the existence of aromatic rings in RhB. The visible absorbance at 554 nm is responsible for the RhB coloration due to the conjugated structure of the C=N and C=O groups. COD removal of the RhB aqueous solution was measured to evaluate the mineralization of RhB. The COD removal efficiency of RhB reached 87.6% in 60 min, indicating that the majority of RhB was mineralized and the H_2A/Fe^0–PS system has a high capacity for degradation of RhB. This result is further confirmed by the UV-vis adsorption spectra of RhB, as shown in Fig. 7. Usually for RhB degradation, two possible competitive mechanisms occur, *i.e.* *N*-demethylation and cleavage of the chromophore structure.[37] First, the decrease in the main chromophore band of RhB at 554 nm with an increase in the reaction time indicates the destruction of the xanthene structure of the chromophore. Second, the decrease in absorbance at 259 nm indicates the destruction of the aromatic part. Third, some new peaks appeared at around 210 nm and 328 nm, possibly demonstrating the yield of intermediate or final products.[38,39]

3.4.3 The role of H_2A in enhancing RhB degradation. The role of H_2A on enhancing RhB degradation in the H_2A/Fe^0–PS system was investigated. First of all, it is generally recognized that H_2A is a potent antioxidant agent with the ability to prevent the aggregation of Fe^0 by the effect of coating (Fig. 2b and d).[40] In addition, H_2A is a weak acid with the ability to solubilize metal ions by Fe^{2+}–H_2A (Fe^{2+}/H_2A_x) complex (eqn (15)) formation either in solution or on the surface of iron based materials, which can not only further activate PS (eqn (16)) and account for the generation of $SO_4^{\bullet-}$, but also react with O_2 to produce $O_2^{\bullet-}$ in accordance with eqn (17).[40] Besides its acidity, H_2A can also serve as a reducing agent, which is capable of effectively reducing Fe^{3+} and realizing Fe^{3+}/Fe^{2+} redox cycles in the system (eqn (18)).

$$Fe^{2+} + H_2A \rightarrow Fe^{2+}H_2A_x \quad (15)$$

$$Fe^{2+}H_2A_x + S_2O_8^{2-} \rightarrow Fe^{3+}H_2A_y + SO_4^{2-} + SO_4^{\bullet-} \quad (16)$$

$$Fe^{2+}H_2A_x + O_2 \rightarrow Fe^{3+}H_2A_y + O_2^{\bullet-} \quad (17)$$

$$H_2A + 2Fe^{3+} \rightarrow Fe^{2+} + A + 2H^+ \quad (18)$$

To confirm this opinion, the changes in concentration of total iron and ferrous iron in the solution were monitored during the oxidation of RhB. Fig. 8 shows that the total iron concentration increased as the reaction time increased, with no period of decline. This phenomenon could be attributed to the continuous leaching of iron from H_2A/Fe^0. By contrast, the leaching of iron was faster during the oxidation of RhB by the H_2A/Fe^0 composite than by pristine Fe^0, and this result further confirms the pronounced weak acid effect of H_2A with the ability to solubilize metal ions. Moreover, the ferrous iron concentration was found to increase from 22.32 to 29.11 mg L^{-1} in the first 20 min, and then remained relatively stable over the later reaction time without decreasing. This was due to the electron transfer from H_2A to both the surface and dissolved Fe^{3+} *via* eqn (18), resulting in an effective Fe^{3+}/Fe^{2+} cycle. As expected, the reductive effect of H_2A was also promoted to form more and more Fe^{2+} and $SO_4^{\bullet-}$ in the H_2A/Fe^0–PS system, which results in an acceleration in RhB degradation.

The H_2A/Fe^0–PS system exhibits significant superiority for the removal of RhB. Fig. 9 illustrates the proposed conceptual model of the RhB removal process by the H_2A/Fe^0–PS system. The superiority of the H_2A/Fe^0–PS system is mainly attributed to: (1) H_2A can reduce the structure size of Fe^0 particles and increase their dispersibility: however, considering that the aggregation of H_2A/Fe^0 was still remarkable (Fig. 2b and d), we

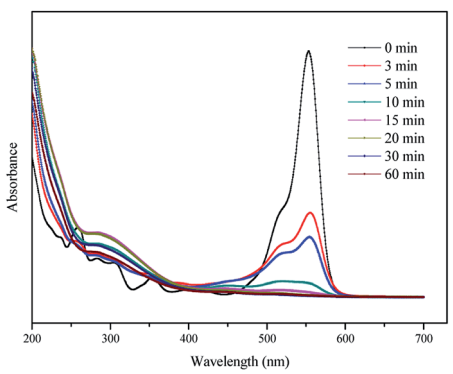

Fig. 7 UV-vis adsorption spectra of RhB at various times by the H_2A/Fe^0–PS system.

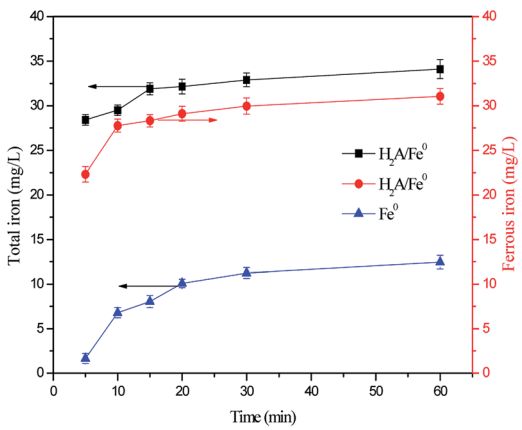

Fig. 8 Variation in total iron and ferrous iron concentrations in solution. Reaction conditions: C_0 = 50 mg L^{-1}, PS = 0.3 g L^{-1}, H_2A/Fe^0 = 0.3 g L^{-1}, pH = 6.50 and T = 298 K.

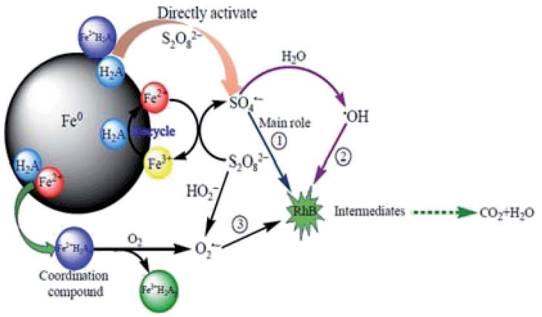

Fig. 9 Conceptual model of the RhB removal process by the H_2A/Fe^0–PS system.

believe that the high activation performance of H_2A/Fe^0 was not mainly due to the increased dispersibility in solution. (2) H_2A is a weak acid that has the ability to solubilize metal ions by Fe^{2+}/H_2A_x complex formation, resulting in another pathway for the production of $O_2^{\cdot-}$ by eqn (17), which is helpful for improving the degradation. (3) H_2A can also serve as a reducing agent, and the presence of H_2A accelerated the redox cycle of Fe^{3+}/Fe^{2+} and robust Fe^{2+} regeneration to promote RhB degradation. Therefore, this H_2A/Fe^0–PS system can produce more $SO_4^{\cdot-}$ and $O_2^{\cdot-}$ than the Fe^0–PS system alone. In a word, the H_2A/Fe^0–PS system involved the generation of $^{\cdot}OH$, $SO_4^{\cdot-}$ and $O_2^{\cdot-}$ species, among which $SO_4^{\cdot-}$ played a key role in the degradation of RhB.

4. Conclusions

In this study, we present H_2A/Fe^0 nanoparticles as a heterogeneous PS activator for the effective degradation of RhB. The physical–chemical properties of H_2A/Fe^0 nanoparticles were characterized by TEM, FE-SEM, FTIR and XPS. Compared with bare Fe^0, the H_2A/Fe^0 composites showed much higher performance for PS activation for RhB degradation. We explored the role of H_2A and concluded that both its reduction and chelating ability contribute to the good performance of the H_2A/Fe^0–PS system. In addition, the radical scavenging tests clearly confirmed the generation of $SO_4^{\cdot-}$, $^{\cdot}OH$ and $O_2^{\cdot-}$ and that the primary reactive oxygen species is $SO_4^{\cdot-}$ in the H_2A/Fe^0–PS system. Batch experiments indicated that the optimal PS dosage is 0.3 g L^{-1}. RhB removal efficiency increased with increasing H_2A/Fe^0 dosage and solution temperature, and it increased with a decrease in pH values. The findings in this study strongly suggested that the H_2A/Fe^0 activated PS process is a highly promising technique for the degradation of dye wastewater and other refractory organic toxic pollutants.

Conflicts of interest

There are no conflicts to declare.

Acknowledgements

The authors gratefully acknowledge the financial support by National Natural Science Foundation of China (NSFC, No. 51368025 and No. 51068011).

References

1 Y. Deng and R. Zhao, *Curr. Pollut. Rep.*, 2015, **1**, 167–176.
2 J. Yan, M. Lei, L. Zhu, M. N. Anjum, J. Zou and H. Tang, *J. Hazard. Mater.*, 2011, **186**, 1398–1404.
3 Y. Fan, Y. Ji, D. Kong, J. Lu and Q. Zhou, *J. Hazard. Mater.*, 2015, **300**, 39–47.
4 J. Y. Fang and C. Shang, *Environ. Sci. Technol.*, 2012, **46**, 8976–8983.
5 G.-D. Fang, D. D. Dionysiou, S. R. Al-Abed and D.-M. Zhou, *Appl. Catal., B*, 2013, **129**, 325–332.
6 X. Zhang, M. Feng, R. Qu, H. Liu, L. Wang and Z. Wang, *Chem. Eng. J.*, 2016, **301**, 1–11.
7 X. Jiang, Y. Wu, P. Wang, H. Li and W. Dong, *Environ. Sci. Pollut. Res. Int.*, 2013, **20**, 4947–4953.
8 C. Wang, J. Wan, Y. Ma and Y. Wang, *Res. Chem. Intermed.*, 2015, **42**, 481–497.
9 F. Gong, L. Wang, D. Li, F. Zhou, Y. Yao, W. Lu, S. Huang and W. Chen, *Chem. Eng. J.*, 2015, **267**, 102–110.
10 X. Wei, N. Gao, C. Li, Y. Deng, S. Zhou and L. Li, *Chem. Eng. J.*, 2016, **285**, 660–670.
11 M. Peluffo, F. Pardo, A. Santos and A. Romero, *Sci. Total Environ.*, 2016, **563–564**, 649–656.
12 J. Yan, L. Han, W. Gao, S. Xue and M. Chen, *Bioresour. Technol.*, 2015, **175**, 269–274.
13 X. Xiong, B. Sun, J. Zhang, N. Gao, J. Shen, J. Li and X. Guan, *Water Res.*, 2014, **62**, 53–62.
14 B. M. Voelker and B. Sulzberger, *Environ. Sci. Technol.*, 1996, **30**, 1106–1114.
15 C. Sun, R. Zhou, J. E, J. Sun, Y. Su and H. Ren, *RSC Adv.*, 2016, **6**, 10633–10640.
16 Y. T. Lin and C. Liang, *Environ. Sci. Technol.*, 2013, **47**, 3299–3307.
17 X. Hou, X. Huang, Z. Ai, J. Zhao and L. Zhang, *J. Hazard. Mater.*, 2016, **310**, 170–178.
18 X.-R. Xu, H.-B. Li, X.-Y. Li and J.-D. Gu, *Chemosphere*, 2004, **57**, 609–613.
19 S. Fukuchi, R. Nishimoto, M. Fukushima and Q. Zhu, *Appl. Catal., B*, 2014, **147**, 411–419.
20 Y.-T. Lin, C. Liang and C.-W. Yu, *Ind. Eng. Chem. Res.*, 2016, **55**, 2302–2308.
21 M. Savasari, M. Emadi, M. A. Bahmanyar and P. Biparva, *J. Ind. Eng. Chem.*, 2015, **21**, 1403–1409.
22 Z.-H. Diao, X.-R. Xu, D. Jiang, L.-J. Kong, Y.-X. Sun, Y.-X. Hu, Q.-W. Hao and H. Chen, *Chem. Eng. J.*, 2016, **302**, 213–222.
23 J. Du, J. Bao, X. Fu, C. Lu and S. H. Kim, *Sep. Purif. Technol.*, 2016, **163**, 145–152.
24 Y. Lei, H. Zhang, J. Wang and J. Ai, *Chem. Eng. J.*, 2015, **270**, 73–79.
25 X. Wang, Y. Du and J. Ma, *Appl. Surf. Sci.*, 2016, **390**, 50–59.
26 X. Wang, P. Wang, J. Ma, H. Liu and P. Ning, *Appl. Surf. Sci.*, 2015, **345**, 57–66.
27 H. Chen, Z. Zhang, M. Feng, W. Liu, W. Wang, Q. Yang and Y. Hu, *Chem. Eng. J.*, 2017, **313**, 498–507.
28 L. Hou, H. Zhang and X. Xue, *Sep. Purif. Technol.*, 2012, **84**, 147–152.

29 C. Tan, N. Gao, W. Chu, C. Li and M. R. Templeton, *Sep. Purif. Technol.*, 2012, **95**, 44–48.
30 Y. Leng, W. Guo, X. Shi, Y. Li and L. Xing, *Ind. Eng. Chem. Res.*, 2013, **52**, 13607–13612.
31 J. Li, Q. Liu, Q. Q. Ji and B. Lai, *Appl. Catal., B*, 2017, **200**, 633–646.
32 C. Tan, N. Gao, Y. Deng, N. An and J. Deng, *Chem. Eng. J.*, 2012, **203**, 294–300.
33 X. Wu, X. Gu, S. Lu, Z. Qiu, Q. Sui, X. Zang, Z. Miao and M. Xu, *Sep. Purif. Technol.*, 2015, **147**, 186–193.
34 A. Farhat, J. Keller, S. Tait and J. Radjenovic, *Environ. Sci. Technol.*, 2015, **49**, 14326–14333.
35 R. Kumar, E. H. Gleissner, E. G. Tiu and Y. Yamakoshi, *Org. Lett.*, 2016, **18**, 184–187.
36 Y. Xu, J. Ai and H. Zhang, *J. Hazard. Mater.*, 2016, **309**, 87–96.
37 J. Hong, S. Lu, C. Zhang, S. Qi and Y. Wang, *Chemosphere*, 2011, **84**, 1542–1547.
38 M. F. Hou, L. Liao, W. D. Zhang, X. Y. Tang, H. F. Wan and G. C. Yin, *Chemosphere*, 2011, **83**, 1279–1283.
39 K. P. Mishra and P. R. Gogate, *Sep. Purif. Technol.*, 2010, **75**, 385–391.
40 X. Hou, W. Shen, X. Huang, Z. Ai and L. Zhang, *J. Hazard. Mater.*, 2016, **308**, 67–74.